INT. J. NUM. METH. HEAT FLUID FLOW, VOL. 2, 21–36 (1992)

MASS ABSORPTION BY ANNULAR LIQUID JETS: III. NUMERICAL STUDIES OF JET COLLAPSE

J. I. RAMOS

Department of Mechanical Engineering, Carnegie Mellon University, Pittsburgh, Pennsylvania 15213-3890, USA

ABSTRACT

A domain-adaptive technique which maps the unknown, time-dependent, curvilinear geometry of annular liquid jets into a unit square is used to determine the steady state mass absorption rate and the collapse of annular liquid jets as functions of the Froude, Peclet and Weber numbers, nozzle exit angle, initial pressure and temperature of the gas enclosed by the liquid, gas concentration at the nozzle exit, ratio of solubilities at the inner and outer interfaces of the annular jet, pressure of the gas surrounding the liquid, and annular jet's thickness-to-radius ratio at the nozzle exit. The domain-adaptive technique yields a system of non-linearly coupled integrodifferential equations for the fluid dynamics of and the gas concentration in the annular jet, and an ordinary differential equation for the time-dependent convergence length. An iterative, block-bidiagonal technique is used to solve the fluid dynamics equations, while the gas concentration equation is solved by means of a line Gauss–Seidel method. It is shown that the jet's collapse rate increases as the Weber number, nozzle exit angle, temperature of the gas enclosed by the annular jet, and pressure of the gas surrounding the jet are increased, but decreases as the Froude and Peclet numbers and annular jet's thickness-to-radius ratio at the nozzle exit are increased. It is also shown that, if the product of the inner-to-outer surface solubility ratio and the initial pressure ratio is smaller than one, mass is absorbed at the outer surface of the annular jet, and the mass and volume of the gas enclosed by the jet increase with time.

KEY WORDS Adaptive method Jet collapse Mass absorption Block-bidiagonal technique, Integrodifferential equations

INTRODUCTION

In Parts I and II[1,2] of this multipart paper, the steady state mass absorption by annular liquid jets was determined as a function of the Froude, Peclet and Weber numbers, pressure difference across the annular jet, nozzle exit angle, and jet thickness-to-radius ratio at the nozzle exit. In order to maintain steady state, mass had to be injected into the volume enclosed by the jet at a rate equal to the mass absorption rate by the liquid.

Two numerical techniques were used to determine the steady state fluid dynamics of annular liquid jets in Part I. The first technique involved the solution of the steady state, Eulerian conservation equations by means of an explicit, fourth-order accurate Runge–Kutta method which was described in Part II. The second technique solved the time-dependent equations by means of the domain-adaptive technique presented in this paper until an asymptotic steady state was reached[3–5].

The domain-adaptive technique employed in Part I maps the curvilinear geometry of the annular jet into a rectangle, and results in an ordinary differential equation for the convergence length which had to be solved iteratively with the fluid dynamics equations.

Line Gauss–Seidel and successive overrelaxation line Gauss–Seidel methods were used in Part I to determine the steady state gas concentration in the annular liquid jet at low and high Peclet numbers using the von Mises transformation.

0961–5539/92/010021–16$2.00

Received March 1991
Revised September 1991

In Part II, the steady state fluid dynamics equations of annular liquid jets were solved by means of an explicit, fourth-order accurate Runge–Kutta method; a linear mapping was introduced to transform the curvilinear geometry of the annular jet into a rectangular one; and, the gas concentration in the liquid was determined by means of a line Gauss–Seidel method at low and high Peclet numbers.

In this paper, a third technique for the solution of the equations governing the fluid dynamics of and the gas concentration in the annular liquid jet is proposed. This technique is based on a domain-adaptive method and the linear mapping introduced in Part II, maps the curvilinear geometry of the annular jet into a fixed square, and can be used to study the steady state mass absorption rate by the liquid and the jet collapse. The steady state is determined asymptotically from the solution of the time-dependent fluid dynamics and gas concentration equations, i.e., the time-dependent equations are solved until a specified steady state convergence criterion is reached. Note that, in steady state, mass must be injected into the volume enclosed by the annular liquid jet at a rate equal to the mass absorption rate. Once a steady state is reached, no mass is injected into the volume enclosed by the jet, which then collapses due to mass absorption.

Since the equations governing the unsteady fluid dynamics of annular liquid jets were presented in Part I[1], the corresponding non-dimensional equations are summarized in the next section where it is shown that the jet collapse is governed by an integrodifferential equation which depends on the mass, pressure and volume of the gas enclosed by the annular jet. Furthermore, since the steady state determined from the technique presented in this paper is the same as those of Parts I and II, Part III only deals with the jet collapse. However, since the jet collapse is an unsteady phenomenon, one cannot use the non-dimensional variables introduced in Parts I and II to derive the non-dimensional gas concentration equation because the concentration at the annular jet's inner interface, and the mass, pressure and volume of the gas enclosed by the jet and the convergence length are functions of time.

The next section deals with the gas concentration in the liquid jet at low Peclet numbers. This equation is non-dimensionalized in the same section where three nondimensional groups are identified. It is shown that the coupling between the fluid dynamics equations and the gas concentration is governed by an integral in the boundary condition at the annular jet's inner interface. The following sections deal with the mass absorption rate by the liquid and with the numerical methods used to solve the non-linearly coupled, integrodifferential equations which govern the fluid dynamics of and the gas concentration in the annular liquid jet, respectively. Results and the Summary conclude the paper.

FLUID DYNAMICS EQUATIONS

The non-dimensional equations governing the fluid dynamics of annular liquid jets were derived in Part I and can be written as:

$$\frac{\partial m}{\partial t}+\frac{\partial}{\partial z}(mu)=0 \tag{1}$$

$$\frac{\partial}{\partial t}(mu)+\frac{\partial}{\partial z}(muu)=\frac{m}{Fr}+\frac{1}{We}\left(\frac{\partial J}{\partial z}-C_{pn}R\frac{\partial R}{\partial z}\right) \tag{2}$$

$$\frac{\partial}{\partial t}(m\bar{v})+\frac{\partial}{\partial z}(mu\bar{v})=\frac{1}{We}\left(C_{pn}R-\frac{\partial J/\partial z}{\partial R/\partial z}\right) \tag{3}$$

$$\bar{v}=\frac{\partial R}{\partial t}+u\frac{\partial R}{\partial z} \tag{4}$$

$$J=R\Big/\left[1+\left(\frac{\partial R}{\partial z}\right)^2\right]^{1/2} \tag{5}$$

$$R_e=R+b/2, \qquad R_i=R-b/2 \tag{6}$$

$$b=R_e-R_i, \qquad R=(R_e+R_i)/2 \tag{7}$$

$$b=\frac{m}{R}\frac{b_0^\star}{R_0^\star} \tag{8}$$

where

$$Fr=u_0^{\star 2}/gR_0^\star, \qquad We=m_0^\star u_0^{\star 2}/2\sigma R_0^\star \tag{9}$$

$$C_{pn}=C_pWe, \qquad C_p=(p_i^\star-p_e^\star)R_0^{\star 2}/m_0^\star u_0^{\star 2} \tag{10}$$

Fr and We are the Froude and Weber numbers, respectively, and C_{pn} denotes the pressure coefficient. Note that Fr and We are constant, and that C_p and C_{pn} may be functions of t because $p_i^\star$ may be a function of t.

Equations (1)–(4) are subject to the following boundary conditions at the nozzle exit[1]:

$$m(t,0)=1, \qquad u(t,0)=1 \tag{11}$$

$$\bar{v}(t,0)=\tan\theta_0, \qquad R(t,0)=1 \tag{12}$$

Note that

$$C_{pn}=\frac{p_e^\star R_0^\star}{2\sigma}\left[\frac{p_i^\star}{p_e^\star}-1\right] \tag{13}$$

where

$$p_i^\star=\frac{M_i^\star \tilde{R} T_i^\star}{\pi R_0^{\star 3}}\left(m_i\Big/\int_0^L R_i^2\,\mathrm{d}z\right), \qquad \frac{p_i^\star}{p_e^\star}=\frac{m_i}{\int_0^L R_i^2\,\mathrm{d}z} \tag{14}$$

$$M_i^\star=\pi R_0^{\star 3}p_e^\star/\tilde{R}T_i^\star, \qquad m_i=m_i^\star/M_i^\star \tag{15}$$

Substitution of (14) into (13) yields:

$$C_{pn}=C_{p\max}\left[m_i\Big/\int_0^L R_i^2\,\mathrm{d}z-1\right] \tag{16}$$

where

$$C_{p\max}=p_e^\star R_0^\star/2\sigma \tag{17}$$

is the ratio of the pressure of the gas surrounding the annular jet to the surface tension of the liquid.

It is clear from (1)–(4) and (16) that the fluid dynamics of annular liquid jets depend on m_i which, in turn, depends on the mass absorption by the liquid and on the mass injected into the volume enclosed by the jet. In the absence of mass injection, m_i depends on the gas absorbed by the liquid as discussed in the next section.

GAS CONCENTRATION IN THE ANNULAR LIQUID JET

Under the assumptions stated in Parts I and II, the gas concentration in the liquid is governed by the following dimensional equations:

$$\frac{\partial u^\star}{\partial z^\star}+\frac{1}{r^\star}\frac{\partial}{\partial r^\star}(r^\star v^\star)=0 \tag{18}$$

$$\frac{\partial c^\star}{\partial t^\star}+u^\star\frac{\partial c^\star}{\partial z^\star}+v^\star\frac{\partial c^\star}{\partial r^\star}=\frac{D^\star}{r^\star}\frac{\partial}{\partial r^\star}\left(r^\star\frac{\partial c^\star}{\partial r^\star}\right)+D^\star\frac{\partial^2 c^\star}{\partial z^{\star 2}} \tag{19}$$

where the stars denote dimensional variables; $v^\star$ is the local radial velocity; $r^\star$ denotes the radial

coordinate measured from the symmetry axis; D^* is the gas–liquid binary diffusion coefficient; and, c^* denotes the gas concentration in the liquid.

Equation (19) is subject to the following boundary conditions[1,2]:

$$c^*(t^*,r^*,0)=c_0^*, \qquad R_i^*(t^*,0)\leqslant r^*\leqslant R_e^*(t^*,0); \qquad u^*\frac{\partial c^*}{\partial r^*}+v^*\frac{\partial c^*}{\partial r^*}=0 \qquad \text{at} \quad z^*=L^* \tag{20}$$

$$c^*[t^*,R_i^*(t^*,z^*),z^*]=p_i^*/H_i, \qquad c^*[t^*,R_e^*(t^*,z^*),z^*]=p_e^*/H_e \tag{21}$$

where c_0^* denotes the gas concentration at the nozzle exit; H_i and H_e denote Henry's constants at the annular jet's inner and outer interfaces, respectively; and L^* is the solution of $R_i^*(t^*,L^*)=0$.

Equation (21) assumes equilibrium at the interfaces. This equilibrium assumption can be justified if the inner and outer surfaces are clean and if the mass absorption rate is not too high for interfacial mass transfer resistance to be important[6,7]. Furthermore, (18) is valid for low void fractions, i.e., when the volume occupied by the gas is much smaller than the volume occupied by the liquid.

Substitution of the non-dimensional concentration:

$$c=\frac{2\tilde{R}T_i^*}{p_e^*}(c^*-p_e^*/H_e) \tag{22}$$

and the following non-dimensional variables:

$$u=u^*/u_0^*, \qquad \bar{v}=\bar{v}^*/u_0^*, \qquad z=z^*/R_0^*, \qquad m=m^*/m_0^* \tag{23}$$

$$b=b^*/R_0^*, \qquad R=R^*/R_0^*, \qquad t=t^*u^*/R_0^*, \qquad r=r^*/R_0^* \tag{24}$$

into (18)–(21), the following system of equations results

$$\frac{\partial u}{\partial z}+\frac{1}{r}\frac{\partial}{\partial r}(rv)=0 \tag{25}$$

$$\frac{\partial c}{\partial t}+u\frac{\partial c}{\partial z}+v\frac{\partial c}{\partial r}=\frac{1}{Pe}\left[\frac{1}{r}\frac{\partial}{\partial r}\left(r\frac{\partial c}{\partial r}\right)+\frac{\partial^2 c}{\partial z^2}\right] \tag{26}$$

$$c(t,r,0)=2\tilde{R}T_i^*S_e\left(\frac{c_0^*}{S_e p_e^*}-1\right), \qquad R_i(t,0)\leqslant r\leqslant R_e(t,0) \tag{27}$$

$$c[t,R_i(t,z),z]=2\tilde{R}T_i^*S_e\left[\frac{S_i}{S_e}\frac{m_i}{\int_0^L R_i^2\,\mathrm{d}z}-1\right] \tag{28}$$

$$c[t,R_e(t,z),z]=0 \tag{29}$$

$$u\frac{\partial c}{\partial z}+v\frac{\partial c}{\partial r}=0 \qquad \text{at} \quad z=L \tag{30}$$

where $S_i=H_i^{-1}$ and $S_e=H_e^{-1}$ denote the solubilities at the annular jet's inner and outer surfaces, respectively, $L=L^*/R_0^*$, and,

$$Pe=u_0^*R_0^*/D^* \tag{31}$$

is the Peclet number.

Equations (27) and (28) and (27) and (29) may be incompatible at $R_i(t,0)$ and $R_e(t,0)$, respectively, i.e., at the annular jet's inner and outer interfaces at the nozzle exit.

MASS ABSORPTION BY THE ANNULAR LIQUID JET

The mass absorption rate at the annular jet inner surface can be written as[1,2].

$$\frac{dm_a^*}{dt} = \int_0^{L^*} 2\pi R_i^* D^* \nabla c^* \cdot \mathbf{n}\, ds^* \tag{32}$$

where $\mathbf{n}$ is the unit vector normal to the inner interface, s is the arc length along the inner interface, and

$$\nabla c^* = \frac{\partial c^*}{\partial r^*}\mathbf{e}_r + \frac{\partial c^*}{\partial z^*}\mathbf{e}_z, \qquad \mathbf{n} = \sin\theta_i \mathbf{e}_z - \cos\theta_i \mathbf{e}_r, \qquad \tan\theta_i^* = \frac{\partial R_i^*}{\partial z^*} \tag{33}$$

$$ds^* = \left[1 + \left(\frac{\partial R_i^*}{\partial z^*}\right)^2\right]^{1/2} dz^* \tag{34}$$

where $\mathbf{e}_r$ and $\mathbf{e}_z$ denote the unit vectors in the r^* and z^* directions, respectively.

Substitution of (33) and (34) into (32) yields:

$$\frac{dm_a^*}{dt^*} = -2\pi D^* \int_0^{L^*} R_i^* \frac{\partial c^*}{\partial r^*}[t^*, R_i^*(t^*, z^*), z^*](1 + \tan^2\theta_i^*)dz^* \tag{35}$$

Substitution of (22)–(24) into (35) yields:

$$\frac{dm_a}{dt} = -\frac{1}{Pe}\int_0^L R_i \frac{\partial c}{\partial r}[t, R_i(t,z), z](1 + \tan^2\theta_i)dz \tag{36}$$

where

$$\tan\theta_i = \frac{\partial R_i}{\partial z}, \qquad m_a = m_a^*/M_i^* \tag{37}$$

If $\partial c/\partial r$ at $[t, R_i(t,z), z]$ is negative, dm_a/dt is positive, and the annular jet absorbs the gas at the rate dm_a/dt. In the absence of mass injection into the volume enclosed by the jet:

$$\frac{dm_i}{dt} = -\frac{dm_a}{dt} = \frac{1}{Pe}\int_0^L R_i \frac{\partial c}{\partial r}[t, R_i(t,z), z](1 + \tan^2\theta_i)dz \tag{38}$$

subject to

$$m_i(0) = \frac{p_i^*(0)}{p_e^*}\int_0^L R_i^2(0,z)dz \tag{39}$$

where (14) has been used.

Equations (1)–(17) and (25)–(39) indicate that, in the absence of mass injection into the volume enclosed by the annular liquid jet, its collapse depends on b_0^*/R_0^*, $C_{p\max}$, Pe, $2\bar{R}T_i^*S_e$, $c_0^*/S_e p_e$, S_i/S_e, Fr, We, θ_0 and $p_i^*(0)/p_e^*$. For the sake of brevity, the following nomenclature will be used hereon

$$\alpha = 2\bar{R}T_i^*S_e, \qquad \beta = c_0^*/S_e p_e^*, \qquad \gamma = S_i/S_e = H_e/H_i \tag{40}$$

Note that α and β are proportional to the temperature of the gas enclosed by the annular liquid jet and the gas concentration at the nozzle exit, respectively, whereas γ represents the ratio of solubilities at the inner and outer interfaces of the annular jet.

NUMERICAL METHODS

Equations (1)–(12) and (25)–(30) represent a system of integrodifferential equations. In order to solve these equations, it is first required to evaluate v, i.e., the local radial velocity, which can be calculated by integrating (25) from $R_i(t,z)$ to r to obtain:

$$vr = v(t,R_i,z)R_i(t,z) - \frac{\partial}{\partial z}\left[u\frac{r^2-R_i^2}{2}\right] - uR_i\frac{\partial R_i}{\partial z} \tag{41}$$

where Leibnitz's rule has been used and u has been assumed to be only a function of t and z. This assumption can be justified, for the gases surrounding and enclosed by the jet have much smaller dynamic viscosities than the liquid and, therefore, they cannot introduce strong velocity variations across the annular jet. This assumption is not valid near the nozzle exit where the liquid relaxes from stick boundary conditions at the nozzle walls to slip/free boundary conditions at the jet interfaces[8]. It is also not valid near the convergence point, i.e., near $z=L$, where a meniscus and an axial pressure gradient exist. Axial and radial pressure gradients were neglected in the derivation of (2) and (3)[8].

Since the inner and outer surfaces of the annular jet are material surfaces,

$$v(t,R_i,z) = \frac{\partial R_i}{\partial t} + u\frac{\partial R_i}{\partial z} \tag{42}$$

$$v(t,R_e,z) = \frac{\partial R_e}{\partial t} + u\frac{\partial R_e}{\partial z} \tag{43}$$

Substitution of (42) into (41) yields:

$$vr = R_i\frac{\partial R_i}{\partial t} - \frac{\partial}{\partial z}\left[u\frac{r^2-R_i^2}{2}\right] \tag{44}$$

and the value of $R_i(=R-b/2)$ can be calculated from (1)–(4) and (8). Furthermore, use of (1) allows to write (4) as:

$$m\bar{v} = \frac{\partial}{\partial t}(mR) + \frac{\partial}{\partial z}(muR) \tag{45}$$

Fluid dynamics equations

Equations (1)–(3) and (45) can be written as:

$$\frac{\partial \mathbf{U}}{\partial t} + \frac{\partial \mathbf{F}(\mathbf{U})}{\partial z} = \mathbf{G} \tag{46}$$

where

$$\mathbf{U} = [m, mR, mu, m\bar{v}]^{\mathrm{T}} \tag{47}$$

$$\mathbf{F} = [mu, mRu, muu, mu\bar{v}]^{\mathrm{T}} \tag{48}$$

$$\mathbf{G} = \left[0, m\bar{v}, \frac{m}{Fr} + \frac{1}{We}\left(\frac{\partial J}{\partial z} - C_{pn}R\frac{\partial R}{\partial z}\right), \frac{1}{We}\left(C_{pn}R - \frac{\partial J/\partial z}{\partial R/\partial z}\right)\right]^{\mathrm{T}} \tag{49}$$

and the superscript T denotes transpose.

Since the annular jet collapse is an unsteady phenomenon, $L=L(t)$ and the non-dimensional physical domain $0 \leqslant z \leqslant L(t)$ is a function of time. This time-dependent physical domain can be transformed into a fixed one by means of the mapping[1,3–5]:

$$(t,z) \rightarrow (\tau,\eta) \tag{50}$$

where

$$\tau = t, \qquad \eta = z/L(t) \tag{51}$$

so that $0 \leqslant \eta \leqslant 1$.

Substitution of (51) into (46) yields:

$$\frac{\partial \mathbf{U}}{\partial \tau} + \frac{1}{L}\left[\mathbf{H} - \eta \frac{\partial L}{\mathrm{d}t}\mathbf{I}\right]\frac{\partial \mathbf{U}}{\partial \eta} = \mathbf{G} \tag{52}$$

where

$$\mathbf{H} = \partial \mathbf{F}/\partial \mathbf{U} \tag{53}$$

and $\mathbf{I}$ is the unit matrix.

Equation (52) can be discretized using backward differences in time and upwind differences in η as[1,3–5]:

$$\left[\mathbf{I} + \frac{\Delta\tau}{\Delta\eta}\mathbf{H}_1\right]_i^{n+1} \mathbf{U}_i^{n+1} - \left[\frac{\Delta\tau}{\Delta\eta}\mathbf{H}_1\right]_i^{n+1} \mathbf{U}_{i-1}^{n+1} = \Delta\tau \mathbf{G}_i^{n+1} + \mathbf{U}_i^n \tag{54}$$

where $\mathbf{U}_i^n = \mathbf{U}(n\Delta\tau, i\Delta\eta)$, $\Delta\tau$ and $\Delta\eta$ denote the time step and the spatial step size, respectively, and,

$$\mathbf{H}_1 = \frac{1}{\mathbf{L}}\left[\mathbf{H} - \eta \frac{\mathrm{d}L}{\mathrm{d}t}\mathbf{I}\right] \tag{55}$$

Equation (54) represents a block bidiagonal matrix which can be easily solved by forward substitution.

Note that $\mathbf{U}$ is known at $i = 1$, i.e.,

$$\mathbf{U}(\tau, 0) = (1, 1, 1, \tan\theta_0)^{\mathrm{T}} \tag{56}$$

where (11) and (12) have been used, and that the terms appearing in $\mathbf{G}$ were discretized using central differences from $i = 2$ to $i = NPI - 1$, where NPI denotes the number of grid points in the η-direction.

At $i = NPI$, i.e., at $\eta = 1$, the terms $\partial R/\partial z$ and $\partial J/\partial z$ that appear in $\mathbf{G}$ (cf. (49)) were discretized as:

$$\left(\frac{\partial R}{\partial \eta}\right)_{NPI} = (R_{NPI} - R_{NPI-1})/\Delta\eta + \mathrm{O}(\Delta\eta) \tag{57}$$

$$\left(\frac{\partial J}{\partial z}\right)_{NPI} = (J_{NPI} - J_{NPI-1})/\Delta\eta + O(\Delta\eta) \tag{58}$$

which represent first-order backward approximations. Calculations were also performed with:

$$\left(\frac{\partial R}{\partial \eta}\right)_{NPI} = (3R_{NPI} + R_{NPI-2} - 4R_{NPI-1})/2\Delta\eta + O(\Delta\eta^2) \tag{59}$$

and yielded almost identical results to (57).

Since (55) depends on $\mathrm{d}L/\mathrm{d}t$ and L, and equation for the convergence length is needed. Such an equation can be obtained from (6) and (8) as follows. At the convergence point $R_i[t, L(t)] = 0$ and (6) implies that:

$$b[t, L(t)] = 2R[t, L(t)] \tag{60}$$

Equation (60) can be substituted into (8) to yield:

$$2R^2[t, L(t)] = b_0^* m[t, L(t)]/R_0^* \tag{61}$$

which can be differentiated with respect to time to yield:

$$4R\left[\frac{\partial R}{\partial t}+\frac{\partial R}{\partial z}\frac{\mathrm{d}L}{\mathrm{d}t}\right]=\frac{b_0^*}{R_0^*}\left[\frac{\partial m}{\partial t}+\frac{\partial m}{\partial z}\frac{\mathrm{d}L}{\mathrm{d}t}\right] \quad \text{at} \quad z=L(t) \tag{62}$$

Equations (1) and (4) can be used to obtain the values of $\partial R/\partial t$ and $\partial m/\partial t$ which can then be substituted into (62) to obtain:

$$\frac{\mathrm{d}L}{\mathrm{d}t}=\frac{\mathrm{d}L}{\mathrm{d}\tau}=\left[-\frac{b_0^*}{R_0^*}\frac{\partial(mu)}{\partial\eta}+4R\left(u\frac{\partial R}{\partial\eta}-\bar{v}L\right)\right]\Bigg/\left[4R\frac{\partial R}{\partial\eta}-\frac{b_0^*}{R_0^*}\frac{\partial m}{\partial\eta}\right] \tag{63}$$

where the right-hand-side of (63) is to be evaluated at $\eta=1$.

Equation (63) represents an ordinary differential equation for L. The partial derivatives with respect to η in (63) can be evaluated using upwind differences as, for example,

$$\frac{\partial m}{\partial\eta}(\tau,1)=(m_{NPI}^{n+1}-m_{NPI-1}^{n+1})/\Delta\eta \tag{64}$$

$$u\frac{\partial R}{\partial\eta}(\tau,1)=u_{NPI}^{n+1}(R_{NPI}^{n+1}-R_{NPI-1}^{n+1})/\Delta\eta \tag{65}$$

the time derivatives can be discretized by means of backward differences, and the resulting non-linear algebraic equation must be solved iteratively together with the finite difference forms of the fluid dynamics and gas concentration equations.

Due to the non-linearity of $\mathbf{H}_1$ and $\mathbf{G}$ and the integrodifferential coupling between the fluid dynamics and gas concentration equations (cf. (16) and (28)), the finite difference forms of (52) and (63) have to be solved iteratively together with the solution of the gas concentration equation (cf. next section) until the following convergence criterion was satisfied:

$$\left[\sum_{i=1}^{NPI}(\mathbf{U}_i^{k+1}-\mathbf{U}_i^k)^{\mathrm{T}}\cdot(\mathbf{U}_i^{k+1}-\mathbf{U}_i^k)\right]^{1/2}\leqslant 10^{-4} \tag{66}$$

where k denotes the kth iteration within the time step.

The solution of (52) and (63) provides the values of m, R, u, $\bar{v}$ and L, and the non-dimensional annular jet thickness can be evaluated by means of (8).

Gas concentration equation

The gas concentration equation (cf. (26)) is to be solved in the time-dependent, curvilinear domain

$$R_i(t,z)\leqslant r\leqslant R_e(t,z), \qquad 0\leqslant z\leqslant L(t) \tag{67}$$

This domain can be transformed into a unit square by means of the map

$$(t,r,z)\rightarrow(\tau,\xi,\eta) \tag{68}$$

where

$$\tau=t, \qquad \xi=(r-R_i)/(R_e-R_i), \qquad \eta=z/L \tag{69}$$

such that $0\leqslant\xi\leqslant 1$ and $0\leqslant\eta\leqslant 1$.

substitution of (69) into (26)–(30) yields (cf. (40)):

$$\frac{\partial c}{\partial\tau}+u_1\frac{\partial c}{\partial\eta}+v_1\frac{\partial c}{\partial\xi}=\frac{1}{Pe}\frac{1}{rb^2}\frac{\partial}{\partial\xi}\left(r\frac{\partial c}{\partial\xi}\right)+\frac{1}{Pe}\left[\frac{1}{L^2}\frac{\partial^2 c}{\partial\eta^2}+\frac{2}{L}\frac{\partial\xi}{\partial z}\frac{\partial^2 c}{\partial\xi\,\partial\eta}+\frac{\partial^2\xi}{\partial z^2}\frac{\partial c}{\partial\xi}+\left(\frac{\partial\xi}{\partial z}\right)^2\frac{\partial^2 c}{\partial\xi^2}\right] \tag{70}$$

$$c(\tau,\xi,0)=\alpha(\beta-1) \tag{71}$$

$$c(\tau,0,\eta)=\alpha\left[\gamma\frac{m_i}{\int_0^L R_i^2\,\mathrm{d}z}-1\right] \tag{72}$$

$$c(\tau,1,\eta)=0 \tag{73}$$

$$\frac{u}{L}\frac{\partial c}{\partial \eta}+\left(u\frac{\partial \xi}{\partial z}+v\frac{\partial \xi}{\partial r}\right)\frac{\partial c}{\partial \xi}=0 \qquad \text{at} \quad \eta=1 \tag{74}$$

where

$$b=R_e-R_i, \qquad r=R_i+\xi b \tag{75}$$

$$u_1=\frac{1}{L}\left[u-\eta\frac{\mathrm{d}L}{\mathrm{d}t}\right] \tag{76}$$

$$v_1=\frac{1}{b}\left\{v-\xi\left[\frac{\partial R_e}{\partial t}+u\frac{\partial R_e}{\partial z}\right]+(\xi-1)\left[\frac{\partial R_i}{\partial t}+u\frac{\partial R_i}{\partial z}\right]\right\} \tag{77}$$

Note that

$$v_1(\tau,0,\eta)=v_1(\tau,1,\eta)=0 \tag{78}$$

because the annular jet inner and outer interfaces are material surfaces (cf. (42) and (43)).

The time derivative and the axial convection terms which appear in (70) were discretized by means of backward differences in time and space, respectively, whereas the remaining terms were discretized by means of second-order accurate finite difference formulae. The resulting finite difference equation involves nine grid points, and was solved by means of a line Gauss–Seidel method by sweeping the computational domain from the nozzle exit to the convergence point as many times as necessary until the convergence criteria of Part I were satisfied. At each axial location, the method of Thomas or tridiagonal matrix algorithm was used to evaluate the gas concentration in the liquid.

Mass absorption rate

The mass absorption rate at the annular jet's inner interface (cf. (36) and (38)) can be written, using (69), as:

$$\frac{\mathrm{d}m_a}{\mathrm{d}t}=-\frac{L}{Pe}\int_0^1\frac{R_i}{b}\frac{\partial c}{\partial \xi}(\tau,0,\eta)[1+\tan^2\theta_i]\mathrm{d}\eta \tag{79}$$

and the integral in (79) was evaluated as:

$$\frac{\mathrm{d}m_a}{\mathrm{d}t}=-\frac{L}{Pe}\sum_{j=2}^{NPI}Q_j\Delta\eta \tag{80}$$

where

$$Q=\frac{R_i}{b}\frac{\partial c}{\partial \xi}(\tau,0,\eta)[1+\tan^2\theta_i] \tag{81}$$

Equation (80) is a rectangular quadrature rule which excludes the contribution of $\partial c(\tau,0,0)/\partial\xi$ to the mass absorption rate. This exclusion is motivated by the fact that there may be mathematical incompatibilities at $(\tau,0,0)$ and $(\tau,1,0)$ due to (27)–(29).

As shown in Part I, if numerical techniques that use the values of $c(\tau,0,0)$ and $c(\tau,1,0)$ are employed to calculate the gas concentration in and the mass absorbed by the liquid, the resulting mass absorption rates may be inaccurate and may not agree with the analytical solutions of the steady state concentration equation. Furthermore, if there are mathematical incompatibilities

at $(\tau,0,0)$ and $(\tau,1,0)$, the gas concentration is not defined and cannot be differentiated with respect to ξ at these points. It is for these reasons that a rectangular quadrature rule was used to calculate the mass absorption rate (cf. (80)) and the gas concentration in the liquid was evaluated by means of an implicit method.

The value of $\partial c/\partial\xi$ in (79) and (81) was evaluated by means of second-order accurate finite difference expressions as, for example,

$$\left(\frac{\partial c}{\partial \xi}\right)_{i,1} = (4c_{i,2} - 3c_{i,1} - c_{i,3})/2\,\Delta\xi + O(\Delta\xi^2) \tag{82}$$

The mass of the gas enclosed by the annular jet was evaluated as (cf. (38)):

$$m_i^{n+1} = m_i^n - \left(\frac{\mathrm{d}m_a}{\mathrm{d}t}\right)^{n+1} + O(\Delta t) \tag{83}$$

The fluid dynamics and gas concentration equations are non-linearly coupled and were solved iteratively until the convergence criteria used in Parts I and II were satisfied.

Initialization

It has been stated throughout the paper that the initial conditions correspond to steady state annular liquid jets for which the mass absorption rate by the liquid is equal to the mass injected into the volume enclosed by the annular jet, i.e.,

$$m_i = m_i(0) \tag{84}$$

and $p_i^\star$ is constant. Therefore, in steady state, the fluid dynamics equations are uncoupled from the gas concentration equation, and (54) can be solved iteratively until the following convergence criterion is satisfied

$$\left[\sum_{i=1}^{NPI} (\mathbf{U}_i^{n+1} - \mathbf{U}_i^n)^{\mathrm{T}} \cdot (\mathbf{U}_i^{n+1} - \mathbf{U}_i^n)/\Delta\tau^2\right]^{1/2} \leqslant 10^{-4} \tag{85}$$

The solution of (54) and (63) together with the steady state convergence criterion defined in (85) provides the values of m, R, u $\bar{v}$, b and L which are used as initial conditions to analyse the annular jet collapse. These initial values can be used to evaluate $m_i(0)$, $L(0)$ and $V(0)$, where V denotes the volume enclosed by the annular jet, i.e.,

$$V = \int_0^L R_i^2\,\mathrm{d}z \tag{86}$$

The steady state concentration in the liquid can be calculated from (70) by setting to zero the derivative with respect to time. The steady state gas concentration in the liquid can then be used as the initial gas concentration to analyze the annular jet collapse which is assumed to start at $\tau=0$. Therefore, the numerical studies of jet collapse presented in this paper consist of two parts. The first part ($\tau\leqslant 0$) corresponds to steady state jets for which the mass absorption rate by the liquid is equal to the mass injection rate into the volume enclosed by the annular jet, and the second part ($\tau>0$) corresponds to the annular jet collapse, i.e., there is no mass injection into the volume enclosed by the jet for $\tau>0$. Needless to say that the results of the first part coincide with those of Parts I and II where the von Mises transformation and a linear mapping, respectively, were used to transform the annular liquid jet geometry into a rectangle.

The steady state analysis used for $\tau\leqslant 0$ is different from that presented in Part I where the von Mises transformation was employed, a time-dependent approach was used to solve the fluid dynamics equations, and the steady state gas concentration was solved by means of implicit techniques. It is also different from that used in Part II where the steady state fluid dynamics

equations were solved by means of an explicit, fourth-order accurate Runge–Kutta method, and the steady state gas concentration in the liquid was solved by means of an implicit technique. Therefore, Parts I, II and III present three different techniques for the numerical evaluation of the steady state fluid dynamics of and the gas concentration in the annular liquid jet. The formulation and numerical methods presented in Part III can also be used to study the collapse of annular jets.

Since Parts I, II and III essentially yield the same steady state mass absorption rates, this paper only deals with the collapse of annular jets.

RESULTS

The number of grid points used to solve the finite difference formulae of the fluid dynamics and gas concentration equations presented in the previous section was varied so as to ensure grid independence. The number of grid points in the axial direction depended on the convergence length: the longer the convergence length, the greater was the number of grid points, *NPI*, used in the axial direction. The value of $\Delta\eta$ was varied from 0.0004 to 0.004, i.e., *NPI* varied from 251 to 2001. These values of $\Delta\eta$ are smaller than those used in Part I, and correspond to smaller values of Δz than those employed in Part II.

The selection of the number of grid points used across the annular jet (*NPJ*) was based on the results of Parts I and II which indicate that, for $Pe=10^5$, $NPJ=1000$ provides mass absorption rates which are nearly independent of the number of grid points *NPJ*. Thus, a value of *NPJ* equal to 1000 was selected for the calculations presented in this paper, and this value corresponds to $\Delta\xi\approx10^{-3}$.

The time step used in the calculations was also selected so as to ensure grid-independent results. It was found that $\Delta\tau=10\cdot\Delta\eta$ yielded almost identical results to $\Delta\tau=\Delta\eta$, and was used in all the calculations presented in this paper. Note that for steady state annular liquid jets in zero gravity, analytical results[9] indicate that $u=1$; therefore, $\Delta\tau=10\cdot\Delta\eta$ corresponds to a Courant number, i.e., $u\,\Delta\tau/\Delta\eta$, of 10. In gravitational environments, u and the Courant number increase as z is increased.

Figure 1 shows that the mass of the gas enclosed by the annular jet decreases as a function of time due to the mass absorbed by the liquid. Since the mass absorption rate decreases as the Peclet number is increased (cf. Part I), the annular jet's collapse rate decreases as the Peclet number is increased. *Figure 1* also indicates that both the pressure coefficient and the mass of the gas enclosed by the annular jet tend to constant asymptotic values which correspond to a zero mass absorption rate. The values of $V/V(0)$ and $L/L(0)$ at $\tau=2.2$ are equal to 0.9546 and 0.9967, respectively, for $Pe=10^4$, and 0.9884 and 0.9993, respectively, for $Pe=10^5$. This means that the both the convergence length and the volume enclosed by the annular liquid jet do not change much during the jet's collapse.

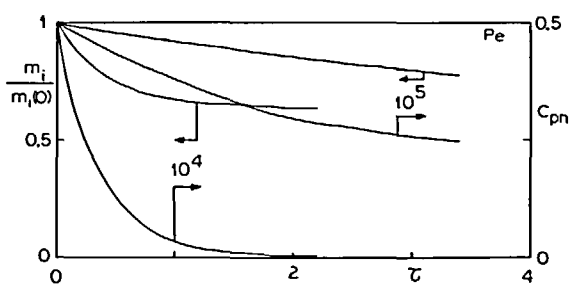

Figure 1 Mass of the gas enclosed by the annular liquid jet and pressure coefficient as functions of time and *Pe*

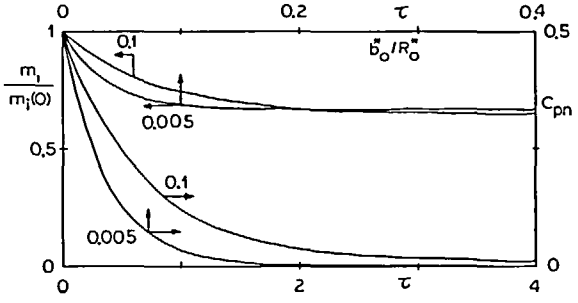

Figure 2 Mass of the gas enclosed by the annular liquid jet and pressure coefficient as functions of time and b_0^*/R_0^*

Figure 2 shows the effect of the annular jet's thickness-to-radius ratio at the nozzle exit on the jet collapse, and indicates that the smaller the value of this ratio, the faster is the jet collapse. This result is consistent with the steady state mass absorption rates shown in Part I, which indicate that the smaller the annular jet's thickness-to-radius ratio at the nozzle exit, the greater is the mass absorption rate. Both the pressure coefficient and the mass of the gas enclosed by the annular liquid jet tend to constant asymptotic values which correspond to zero mass absorption rates. The time at which the asymptotic values are achieved depends on the annular jet's thickness-to-radius ratio at the nozzle exit, i.e., the smaller the value of b_0^*/R_0^*, the shorter is the time required to achieve zero mass absorption rates.

Although not shown in *Figure 2*, both the pressure coefficient and the mass of the gas enclosed by the annular jet corresponding to $b_0^*/R_0^*=0.05$ are nearly identical to those corresponding to $b_0^*/R_0^*=0.1$. The values of $V/V(0)$ and $L/L(0)$ at $\tau=2.2$ are 0.9644 and 0.9982, respectively, for $b_0^*/R_0^*=0.1$; 0.9546 and 0.9967, respectively, for $b_0^*/R_0^*=0.05$; and, 0.9995 and 1.0000, respectively, for $b_0^*/R_0^*=0.005$.

Figure 3 shows the effect of the Froude number on the jet collapse, and indicates that the annular jet's collapse rate increases as the Froude number is decreased. This result is consistent with those presented in Part I which show that the steady state mass absorption rate decreases as the Froude number is increased, i.e., as the convergence length decreases.

Although not shown in *Figure 3*, both the mass of the gas enclosed by the annular jet and the pressure coefficient corresponding to $Fr=\infty$ are nearly identical to those corresponding to $Fr=1000$. This result is consistent with those presented in Part I which indicate that both the steady state mass absorption rate and the steady state convergence length are nearly independent of the Froude number for $Fr\geqslant 1000$. The values of $V/V(0)$ and $L/L(0)$ at $\tau=1.4$ are 0.9832 and 0.9995, respectively, for $Fr=10$; 0.9898 and 1.0000, respectively, for $Fr=1000$; and, 0.9896 and 1.0000, respectively, for $Fr=10^{31}$.

Figure 4 indicates that the jet collapse rate increases as the Weber number is decreased. As shown in Part I, the steady state mass absorption rate increases as the Weber number is increased. Note that an increase in the Weber number corresponds to an increase in the steady state convergence length. The values of $V/V(0)$ and $L/L(0)$ at $\tau=2.0$ are 0.8373 and 0.9336, respectively, for $We=5$; 0.9629 and 0.9977, respectively, for $We=50$; and, 0.9723 and 0.9986, respectively, for $We=75$.

Figure 5 shows the mass of the gas enclosed by the annular liquid jet and the pressure coefficient as functions of the nozzle exit angle and time, and indicates that the jet's collapse rate increases as the nozzle exit angle is decreased from zero.

The steady state mass absorption rates presented in Part I indicate that the mass absorption rate is smaller for $\theta_0=-30$ than for $\theta_0=0$, whereas the results presented in *Figure 5* indicate that the jet's collapse rate is faster for $\theta_0=-30$ than for $\theta_0=0$. The values of $V/V(0)$ and $L/L(0)$ at $\tau=1.0$ are equal to 0.9957 and 0.9989, respectively, for $\theta_0=-30$; and, 0.9924 and 0.9999, respectively, for $\theta_0=0$.

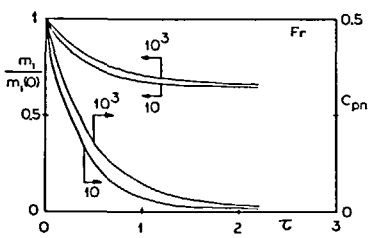

Figure 3 Mass of the gas enclosed by the annular liquid jet and pressure coefficient as functions of time and *Fr*

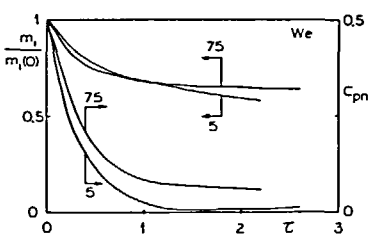

Figure 4 Mass of the gas enclosed by the annular liquid jet and pressure coefficient as functions of time and *We*

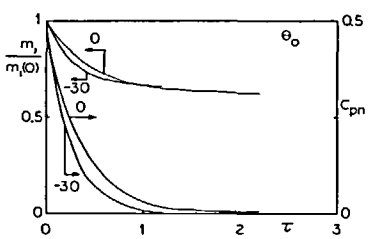

Figure 5 Mass of the gas enclosed by the annular liquid jet and pressure coefficient as functions of time and θ_0

Figure 6 shows the effect of the initial pressure of the gas enclosed by the annular liquid jet on the jet collapse. For $p_i^*(0)/p_e^* = 1$ and the values of the parameters shown in *Table 1*, both the mass of the gas enclosed by the annular jet and the pressure coefficient are identical to their initial values, i.e., $m_i(0) = 1$ and $C_{pn} = 0$. The mass of the gas enclosed by the annular jet and the pressure coefficient decrease and increase for overpressurized and underpressurized jets, respectively. For both overpressurization and underpressurization, m_i and C_{pn} tend to constant asymptotic values, and C_{pn} tends to zero. Note that m_i at $\tau = 3$ is nearly twice the value of $m_i(0)$ for $p_i^*(0)/p_e^* = 0.5$.

The values of $V/V(0)$ and $L/L(0)$ at $\tau = 2.4$ are 0.9457 and 0.9955, respectively, for $p_e^* = 1.5$; 1.0000 and 1.0000, respectively, for $p_i^*(0)/p_e^* = 1.0$; and, 1.0496 and 1.0058, respectively, for $p_i^*(0)/p_e^* = 0.5$.

Figure 7 illustrates the effect of C_{pmax} on the jet collapse, and indicates that the collapse rate increases as C_{pmax} is increased. *Figure 7* also shows that if the time step is not small enough, C_{pn} exhibits the growing behaviour illustrated by broken lines in the Figure. These broken lines correspond to $\Delta\tau = 0.04$. For $\Delta\tau = 0.0004$, the C_{pn} curves corresponding to $C_{pmax} = 5$ and 10 nearly fall on the same curve as that corresponding to $C_{pmax} = 1$. It must be indicated that, for example, $10\times$ indicates that the scale of C_{pn} shown in the right of *Figure 7* is to be reduced by a factor of 10. The values of $V/V(0)$ and $L/L(0)$ at $\tau = 2.6$ are 0.9944 and 0.9994, respectively, for $C_{pmax} = 1$; 0.9713 and 0.9970, respectively, for $C_{pmax} = 5$; and, 0.9413 and 0.9944, respectively, for $C_{pmax} = 10$.

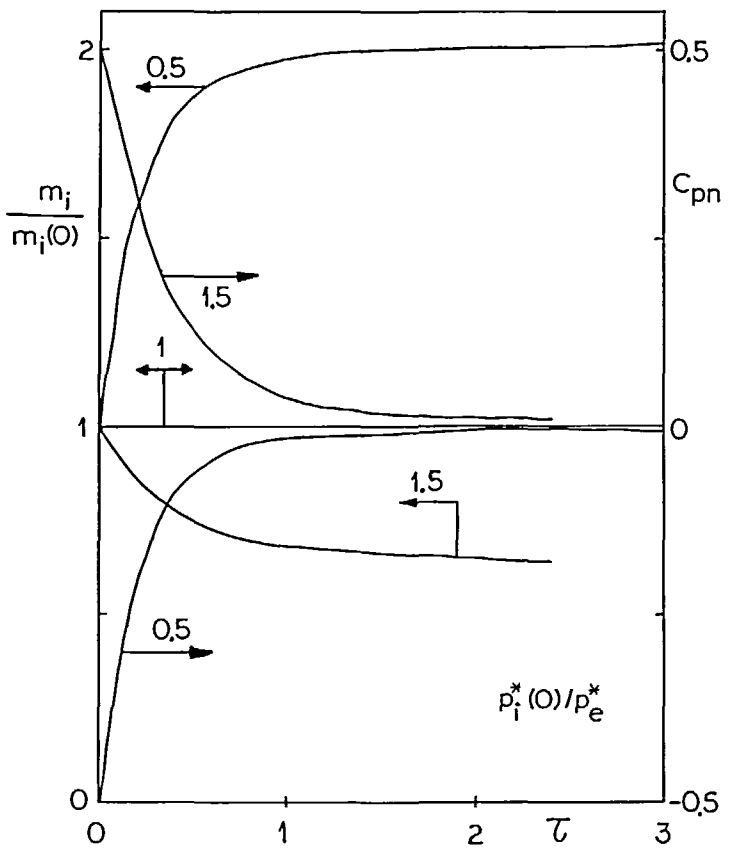

Figure 6 Mass of the gas enclosed by the annular liquid jet and pressure coefficient as functions of time and $p_i^*(0)/p_e^*$

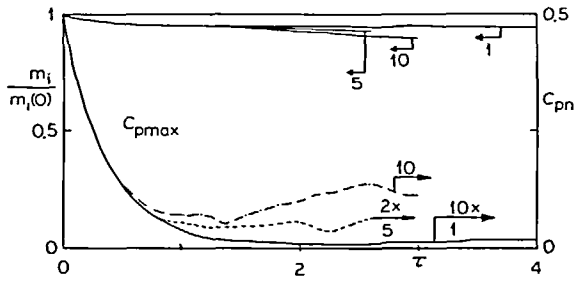

Figure 7 Mass of the gas enclosed by the annular liquid jet and pressure coefficient as functions of time and C_{pmax}

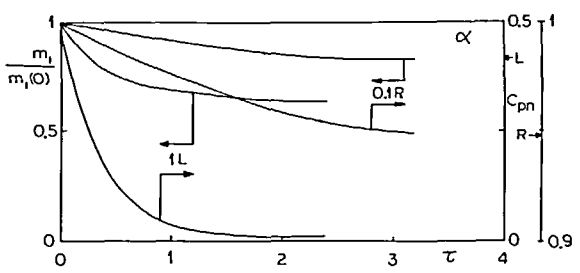

Figure 8 Mass of the gas enclosed by the annular liquid jet and pressure coefficient as functions of time and α

Figure 8 shows the effect of α on the jet collapse, and indicates that the annular jet's collapse rate increases as α is decreased. Note that two scales for the pressure coefficient are presented in *Figure 8*. The right scale (R) is to be used with $\alpha=0.1$, whereas the left scale (L) must be used with $\alpha=1$. The values of $V/V(0)$ and $L/L(0)$ at $\tau=2.4$ are 0.9852 and 0.9991, respectively, for $\alpha=0.1$; and, 0.9457 and 0.9955, respectively, for $\alpha=1.0$.

Figure 9 indicates that the annular jet's collapse rate is nearly independent of the value of β, i.e., it is nearly independent of the gas concentration at the nozzle exit. This result indicates that the gas concentration at the annular liquid jet's inner interface which is initially equal to 0.5 for the values of the parameters shown in *Table 1* is the controlling factor on the jet's collapse. Note that the steady state mass absorption rate increases as β is increased if the gas concentration at the annular liquid jet's inner interface is zero. The values of $V/V(0)$ and $L/L(0)$ at $\tau=2.4$ are 0.9457 and 0.9955, respectively, for $\beta=0$, 10 and 100.

Figure 10 shows the effect of the solubility ratio on the jet collapse, and indicates that if the solubility ratio is equal to 0.1, both the pressure of the gas enclosed by the annular liquid jet and the pressure coefficient increase with time because the gas diffuses from the outer to the inner interface. If the solubility ratio is equal to ten, mass is absorbed by the liquid, and both the mass enclosed by the annular liquid jet and the pressure coefficient decrease with time. It must be noted that the initial concentration at the annular jet's inner interface depends on α, γ and $p_i^*(0)/p_e^*$ (cf. (16), (28) and (40)), and that it $\gamma p_i^*(0)/p_e^*=1$, the initial concentration at the inner interface is zero. Therefore, if $\gamma p_i^*(0)/p_e^*$ is greater than one, the annular jet will collapse due to mass absorption, whereas if $\gamma p_i^*(0)/p_e^*$ is less than one, the non-dimensional gas concentration at the annular jet's inner interface is negative, the gas diffuses from the outer to

Table 1 Values of the parameters used in the calculations

Figure	*Pe*	b_0^*/R_0^*	*Fr*	*We*	θ_0	$p_i^*(0)/p_e^*$	C_{pmax}	α	β	γ
1	var.[a]	0.05	10	50	0	1.5	1	1	0	1
2	10^4	var.	10	50	0	1.5	1	1	0	1
3	10^4	0.05	var.	50	0	1.5	1	1	0	1
4	10^4	0.05	10	var.	0	1.5	1	1	0	1
5	10^4	0.05	10	50	var.	1.5	1	1	0	1
6	10^4	0.05	10	50	0	var.	1	1	10	1
7	10^4	0.05	10	50	0	1.05	var.	1	0	1
8	10^4	0.05	10	50	0	1.5	1	var.	0	1
9	10^4	0.05	10	50	0	1.5	1	1	var.	1
10	10^4	0.05	10	50	0	1.5	1	1	0	var.

[a] var. = variable

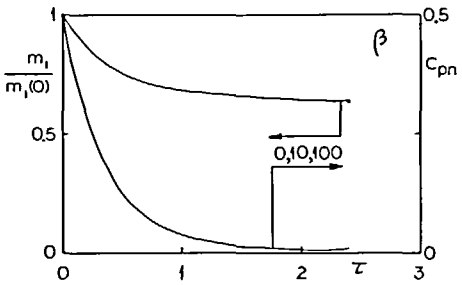

Figure 9 Mass of the gas enclosed by the annular liquid jet and pressure coefficient as functions of time and β

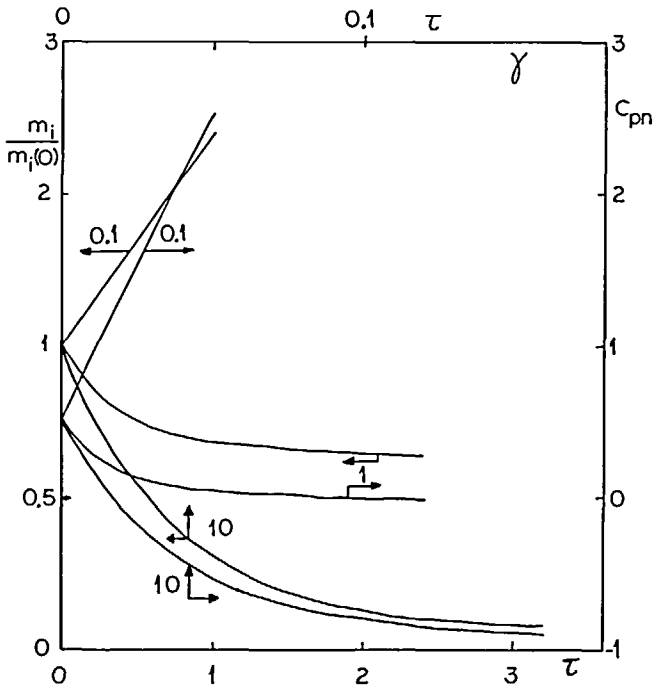

Figure 10 Mass of the gas enclosed by the annular liquid jet and pressure coefficient as functions of time and γ

the inner interface of the annular liquid jet, and the mass of the gas enclosed by the annular liquid jet increases with time.

The values of $V/V(0)$ and $L/L(0)$ at $\tau=0.4$ are 1.0000 and 1.0017, respectively, for $\gamma=0.1$; 0.9457 and 0.9955, respectively, for $\gamma=1$; and, 0.9948 and 1.0000, respectively, for $\gamma=10$.

CONCLUSIONS

A domain-adaptive technique which transforms the time-dependent, curvilinear geometry of annular liquid jets into a unit square has been used to study the collapse of annular liquid jets as a function of the binary gas–liquid diffusion coefficient, gravitational force, surface tension of the liquid, nozzle exit angle, temperature of the gas enclosed by the annular liquid jet, gas concentration at the nozzle exit, pressure of the gas surrounding the liquid, annular jet's thickness-to-radius ratio at the nozzle exit, and solubilities of the gases that surround and are enclosed by the annular jet.

It is shown that the jet collapse is governed by a system of integrodifferential equations which depend on the unknown location of the convergence point, i.e., the point at which the annular jet merges on the symmetry axis to form a solid jet, and that the convergence length is given by an algebraic equation which can be transformed into an ordinary differential equation in time. The annular jet's collapse rate increases as the Weber number, nozzle exit angle, temperature of the gas enclosed by the annular jet, and pressure of the gas which surrounds the annular jet are increased, but decreases as the Froude and Peclet numbers and annular jet's thickness-to-radius ratio at the nozzle exit are increased. If the initial pressure of the gas enclosed by the annular

liquid jet is higher than the pressure of the gas which surrounds the jet, the collapse rate is independent of the gas concentration at the nozzle exit for the values of the parameters analyzed in this paper. The ratio of the solubility of the gas enclosed by the jet to the solubility of the gas which surrounds the jet, and the ratio of the initial pressure of the gas enclosed by the annular jet to the pressure of the gas which surrounds the jet play an important role on the jet collapse. If the product of these ratios is greater than one, the gas diffuses from the inner to the outer interface of the annular liquid jet and the mass of the gas enclosed by the jet decreases with time. However, if the product of these ratios is less than one, the gas diffuses from the outer to the inner interface, and the mass of the gas enclosed by the annular jet increases with time. It has also been found that both the convergence length and the volume enclosed by the annular jet do not change much during the jet collapse because the gas enclosed by the jet was assumed to be isothermal.

ACKNOWLEDGEMENTS

The calculations presented in this paper were performed at the Facultad de Informatica/Escuela Tecnica Superior de Ingenieros de Telecomunicacion of the University of Malaga, Spain. The author is most grateful to Mr. Juan Falgueras for his help with the preparation of this paper.

REFERENCES

1 Ramos, J. I. Mass absorption by annular liquid jets: I. Analytical and numerical studies using the von Mises transformation, *Int. J. Num. Meth. Heat Fluid Flow*, **1**, 99–120 (1991)
2 Ramos, J. I. Mass absorption by annular liquid jets: II. Analytical and numerical studies using a linear mapping, *Int. J. Num. Meth. Heat Fluid Flow*, **1**, 121–141 (1991)
3 Ramos, J. I. and Pitchumani, R. Dynamics of liquid membranes. I: Non-adaptive finite difference methods, *Int. J. Num. Meth. Fluids*, **12**, 859–879 (1991).
4 Ramos, J. I. Dynamics of liquid membranes. II: Adaptive finite difference methods, *Int. J. Num. Meth. Fluids*, **12**, 881–894 (1991)
5 Ramos, J. I. Dynamic response of liquid curtains to time-dependent pressure fluctuations, *Appl. Math. Modelling* **15**, 126–135 (1991)
6 Cussler, E. L. *Diffusion: Mass Transfer in Fluid Systems*, Cambridge University Press, New York, pp. 242–245 (1984)
7 Bird, R. B., Stewart, W. E. and Lightfoot, E. M. *Transport Phenomena*, John Wiley, New York, pp. 652–656 (1960)
8 Ramos, J. I. Liquid membranes: formulation and steady state analysis, *Report CO/89/4*, Department of Mechanical Engineering, Carnegie Mellon University, Pittsburgh (February 1989)
9 Ramos, J. I. Annular liquid jets in zero gravity, *Appl. Math. Modelling*, **14**, 630–640 (1990)